Focus-Scanning Leaky-Wave Antenna With Electronically Pattern-Tunable Scatterers

Yasuaki Monnai, *Student Member, IEEE*, and Hiroyuki Shinoda, *Member, IEEE*

***Abstract*—A focus-scanning leaky-wave antenna is proposed. It is based on evanescent wave scattering by electronically pattern tunable scatterers fabricated of fine cascade connections of field effect transistors (FETs). The focus is tailored by switching the FETs so that numbers of the scattered waves cause constructive interference at the target point. Our prototype achieved focus-scanning at 2.4 GHz. The proposed antenna can be used as a very low-cost and lightweight phased array especially suitable to indoor use.**

***Index Terms*—Evanescent waves, focused antennas, focus-scanning, leaky-wave antennas, phased arrays, reconfigurable microstrip arrays.**

I. Introduction

FOCUSED microwave transmission and reception with phased array technique is a fundamental solution to various kinds of up-to-date microwave challenges in indoor situations, for example, throughput increase of wireless communications, passive radar detection of distributed wireless devices such as RFID tags and wireless LAN nodes, securing high electromagnetic compatibility (EMC), and reducing human exposure to microwaves. In order to transmit focused waves in a room, the size of the aperture has to be comparable to the room scale (typically 1–2 m in length). Although several near-field focused antennas using microstrip arrays have been developed recently [1]–[4], they have been designed only for a fixed focus. Steering the focus with numbers of phase shifters requires expensive and bulky system for those purposes. As a result, the use of phased arrays that cover indoor spaces has been impractical.

In this paper, we propose a novel focus-scanning antenna with a large aperture which can be fabricated in a thin and light body at low cost without phase shifters. It works based on evanescent wave scattering by reconfigurable microstrip array fabricated of field effect transistors (FETs). Fig. 1 illustrates the concept. The structure consists of a waveguide layer and a scatterer layer. The waveguide is a kind of microstrip lines with an inductive surface and supports an evanescent wave. On the top of the inductive surface, there is a microstrip line-based fine cascade connection of FET source-drain channels that works as reconfigurable microstrip array by switching the gate-source voltages. When a microstrip dipole (or a scatterer) is formed on the surface, it scatters a portion of the evanescent wave into the air in a phase ranging from 0 to 2π depending on its location. Therefore, a focus is tailored by tuning the scatterer pattern so that numbers of the scattered waves cause constructive interference at the target point. The focus can be scanned rapidly in the xz-plane by switching the FETs with quite low voltage and little idle current. The formed focus is effective both on transmitting and receiving. We have proposed the original concept recently in [5] and carried out some simulations there. Here we fabricate a real device and demonstrate microwave focus-scanning at 2.4 GHz with focal width of one-wavelength at a distance of five-wavelength above the waveguide.

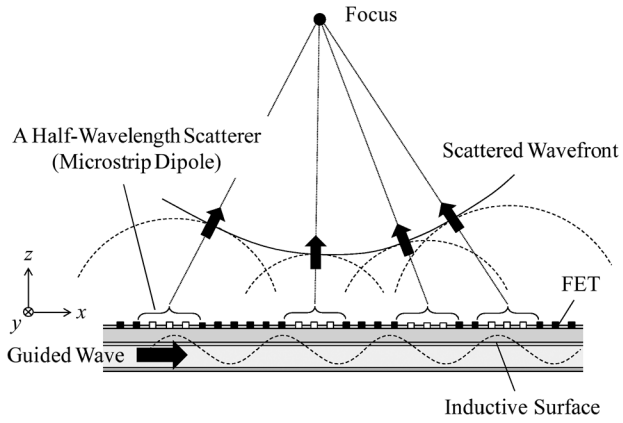

Fig. 1. Concept of focused radiation by the electronically tunable scatterer pattern. The on (off) state of each FET is shown in white (black). Half-wavelength series of on-state regions works as one scatterer because a microstrip dipole is formed.

II. Beam-Steering Leaky-Wave Antennas

The proposed antenna can be classified as a kind of leaky-wave antennas because it is based on coherent energy leakage from a perturbed waveguide. The important difference from the traditional leaky-wave antennas consists in the feasibility of focus-scanning. Although most of the conventional periodic leaky-wave antennas are good at far-field beam-steering by varying the operating frequency [6]–[8] or by tuning the effective permeability/permittivity of the waveguide

Manuscript received May 02, 2010; revised August 31, 2010; acceptance October 20, 2010. Date of publication April 19, 2011; date of current version June 02, 2011. The research was supported in part by a Grant-in-Aid for the JSPS Fellows (22-4238), National Institute of Information and Communications Technology (NICT) 13701 and in part by the Murata Science Foundation.

The authors are with the Department of Information Physics and Computing, University of Tokyo, Tokyo 113-8656, Japan (e-mail: monnai@alab.t.u-tokyo.ac.jp).

Color versions of one or more of the figures in this paper are available online at http://ieeexplore.ieee.org.

Digital Object Identifier 10.1109/TAP.2011.2143680

media [9]–[11], they have difficulty in near-field focusing because periodic scatterers produce only linearly tilted wavefront whereas focusing requires converging wavefront. In contrast, our structure radiates converging wavefront with a fixed-waveguide perturbed by tunable non-periodic scatterers.

Several beam-steering leaky-wave antennas that have been proposed recently without fixed gratings [12]–[14] are of importance to note here because they are potentially able to implement focusing. Sievenpiper [12] demonstrated forward and backward beam-steering based on leaky-wave scattering by non-uniformly modulated surface impedance on a textured high-impedance surface incorporating varactor diodes. Although it was mentioned as a kind of "steerable planar lens", it was not applied to focusing in the literature. Compared to their structure, ours has a separate waveguide layer and scatterer layer, and both of them can easily be fabricated into a printed structure. A structure proposed by Huang *et al.* [13] is more similar to ours in that it uses a fixed-waveguide perturbed by separate switchable gratings. They developed an electronically switchable grating fabricated of p-i-n diode array aligned in parallel in two different periods along the surface of a dielectric waveguide. In the literature, the entire array was controlled by a common bias voltage and therefore only two beam angles could be switched. In oder to tailor various radiation patterns, much more p-i-n diodes are required and each of their bias voltage has to be controlled independently. However, more p-i-n diodes involve more idle current. Lim *et al.* [14] proposed a different concept. They controlled the beamwidth of leaky-wave by superposing different angle leaky-waves in a way that the propagation constant varied non-uniformly in each part a composite right/left-handed (CRLH) transmission line incorporating varactor diodes. This approach requires numbers of voltage controllers to tune the individual varactor diode continuously. While the literature demonstrated the beamwidth control of diverging waves, they did not discuss converging waves.

III. Proposed Structure

A. Waveguide With an Inductive Surface

First of all, we consider a parallel plate waveguide consisting of an inductive surface and a ground plane insulated by a dielectric substrate as shown in Fig. 2(b). Note that Fig. 2(b) also illustrates the FET array and the FR-4 substrate added on the waveguide surface. An inductive surface can easily be fabricated with metal mesh whose lattice constant is sufficiently finer than the wavelength [16], [17]. When a microwave is guided in the x-direction, most power flows inside the waveguide while the rest flows along the inductive surface as an evanescent wave. When the dielectric substrate is thin enough, the E_z component of the dominant TM mode right above the inductive surface is described as follows [17].

$$E_z = \frac{\beta^2}{\alpha} V e^{-\alpha z} e^{-j(k_g x - \omega t)} (z > 0) \tag{1}$$

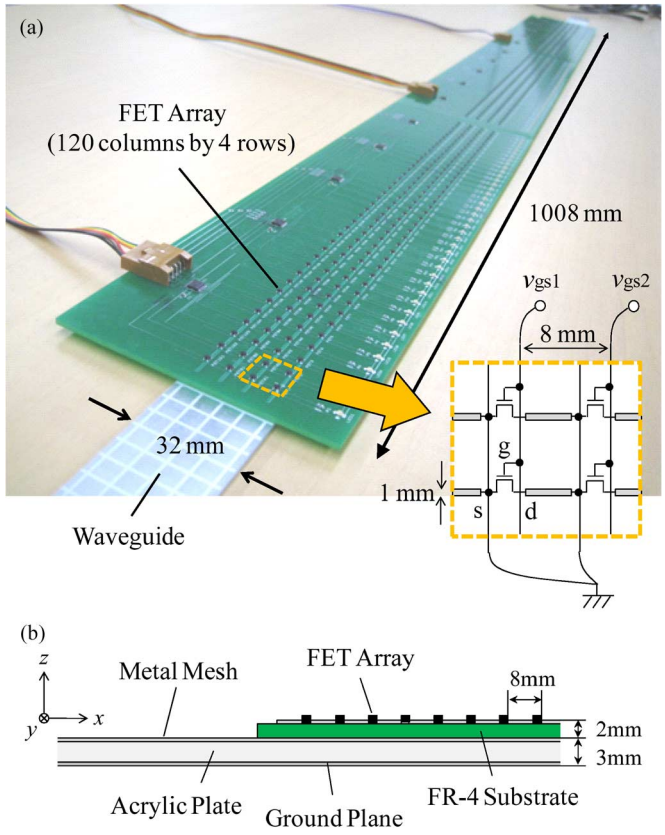

Fig. 2. (a) Photograph of the fabricated structure. (b) Cross-sectional image.

$$\begin{cases} k_g = \sqrt{\varepsilon_s k_a^2 - \frac{j\eta\varepsilon_0\varepsilon_s\omega}{t_s}} \\ \alpha = \sqrt{k_g^2 - k_a^2} \\ \beta = \sqrt{-k_g^2 + \varepsilon_s k_a^2} \end{cases} \tag{2}$$

where V is the voltage between the two plates, ω is the angular frequency, $k_a \equiv \varepsilon_0\mu_0\omega^2$ is the wavenumber in the free space where ε_0 and μ_0 are the permittivity and permeability of the free space, respectively, ε_s is the relative permittivity of the dielectric substrate, t_s is the thickness of the dielectric substrate, and η is the surface impedance of the inductive surface. Since the surface is inductive, η is an imaginary quantity with a positive imaginary part. According to (2), it makes the wavenumber, k_g, a little bit larger than that of a parallel plate waveguide with a flat metal surface which is given by $\sqrt{\varepsilon_s}k_a$.

B. Reconfigurable Microstrip Arrays

The proposed pattern-tunable scatterer array in close proximity to the inductive surface is fabricated of microstrip line-based fine cascade connection of FET source-drain channels each of whose conductivity is switchable by the gate-source voltages as shown in Fig. 2(a). The scattering principle is explained as follows. If the source-drain channels are insulated (off-state), the microstrip lines are unlinked and chopped so short that they have little influence on the traveling evanescent wave. However, when some of the serial channels become conductive (on-state), the chopped lines are linked to form a longer

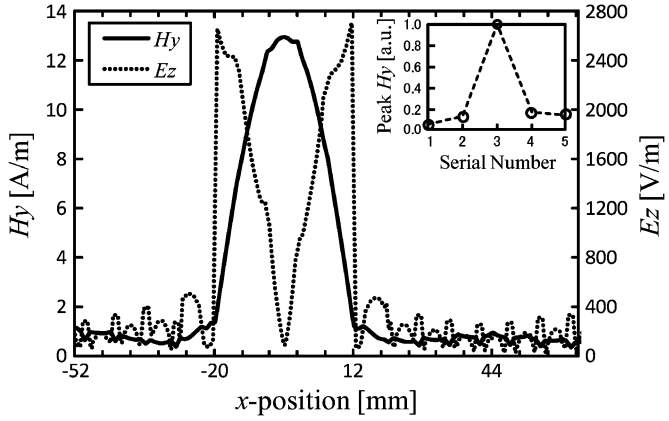

Fig. 3. Simulated field profile at 1 mm below the FET array. The linked line is located at $-20 \leq x \leq 12$ mm. The inset describes the amplitude of H_y as a function of the serial number of the shorted spacings.

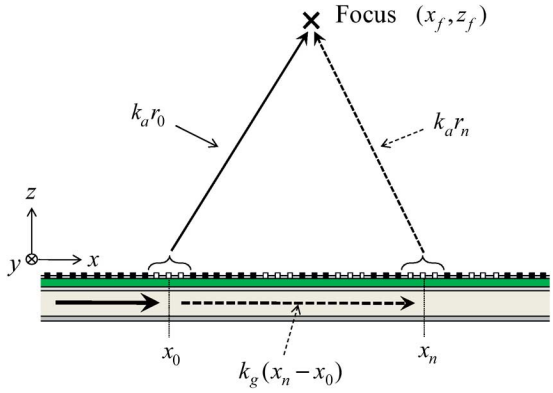

Fig. 4. Focusing situation. A scatterer (in white) radiates a portion of the guided wave in a location-dependent phase delay. A focus is formed when scattered waves cause a constructive interference at the target point.

microstrip line, on which currents are induced by the evanescent wave. In particular, when the linked line gets close to the half-wavelength, it works as a scatterer because a microstrip dipole is formed due to the current resonance. Therefore, the scatterer pattern can be programmed by switching each FET in order to form half-wavelength lines at arbitrary positions as conceptually illustrated in Fig. 1. A microstrip dipole is not a good radiator unless the dielectric substrate is thick enough [18]. Meanwhile, maximizing the radiation efficiency of each radiator is not a purpose here, rather, each radiation should be weak in order to feed as many scatterers as possible and obtain a large aperture.

We show a simulation on the reconfigurable microstrip dipole with MW-Studio (CST). The structure was modeled based on Fig. 2. The on-state (off-state) of a source-drain channel was simply modeled by a short (open) of a chopped microstrip line spacing. At first, we excited a guided wave with all the spacings opened (i.e. no scatterers), from which the guided wavelength, λ_g, was estimated to be about 70 mm at 2.4 GHz. Then, we next shorted 3 serial spacings in order to link the 4 chopped lines of 32 mm long ($\simeq \lambda_g/2$), and excited a guided wave again. Fig. 3 plots the simulated amplitude profiles of the magnetic field (H_y) and the electric field (E_z) at 1 mm below the FET array (i.e. 1 mm above the waveguide surface), where the linked line is located in $-20 \leq x \leq 12$ mm. H_y is strong at the center of the line while E_z is strong at the edges of the line. The sign of E_z was opposite for the both edges (not shown). The inset in Fig. 3 describes the peak amplitude change of H_y as a function of the serial number of the shorted spacings. A remarkable increase is observed at the 3 series. These results certify the resonance of the evanescent wave-induced current on the linked line and the formation of a microstrip dipole. Choosing other numbers of the shorted spacings will lead to operation at other frequency bands.

C. Near-Field Focusing

In this section, we derive scatterer patterns required for focusing. A focus is formed when numbers of scattered waves cause constructive interference at the focal point. For simplicity, we assume each scattering is isotropic. Considering the situation illustrated in Fig. 4, the constructive interference occurs when the following condition is satisfied.

$$k_g(x_n - x_0) + k_a(r_n - r_0) = 2\pi n \quad (n = 0, 1, \cdots) \tag{3}$$

where x_n is the x-position of the n-th scatterer, and r_n is the distance from $(x_n, 0)$ to the focus at (x_f, z_f) given as

$$r_n = \sqrt{(x_f - x_n)^2 + z_f^2}. \tag{4}$$

From (3), we obtain the following solution

$$x_n = \frac{-b_n - \sqrt{b_n^2 - ac_n}}{a} \tag{5}$$

where

$$\begin{cases} a = k_g^2 - k_a^2 \\ b_n = -2k_g n\pi - k_g^2 x_0 + k_a^2 x_f - k_a k_g \sqrt{(x_0 - x_f)^2 + z_f^2} \\ c_n = 4n\pi(n\pi + k_g x_0) + \left(k_a^2 + k_g^2\right) x_0^2 \\ \qquad -2k_a^2 x_0 x_f + 2k_a(2n\pi + k_g x_0)\sqrt{(x_0 - x_f)^2 + z_f^2} \end{cases} \tag{6}$$

(5) yields a quasi-periodic pattern as shown in the following section in Fig. 8(ii). Note that the calculated x_n must be discretized by the period of the FET array, which also means that the FETs have to be aligned sufficiently finer than the guided wavelength. The location of the first scatterer, x_0, can be chosen arbitrarily based on experimental convenience.

The radiation pattern is calculated by superposing each scattered wave.

$$\varphi(x, z) = \sum_n \alpha_n \frac{e^{-j(k_g x_n + k_a R_n(x,z))}}{R_n(x, z)} \tag{7}$$

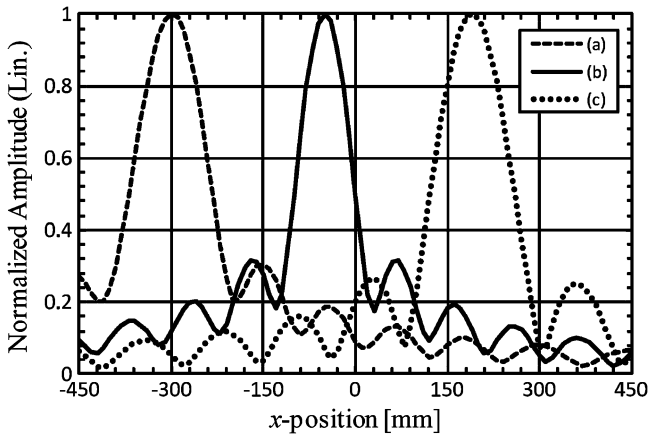

Fig. 5. Theoretical near-field pattern. The focus is designed for (a) $(-300, 600)$ mm, (b) $(-50, 500)$ mm, and (c) (200, 900) mm.

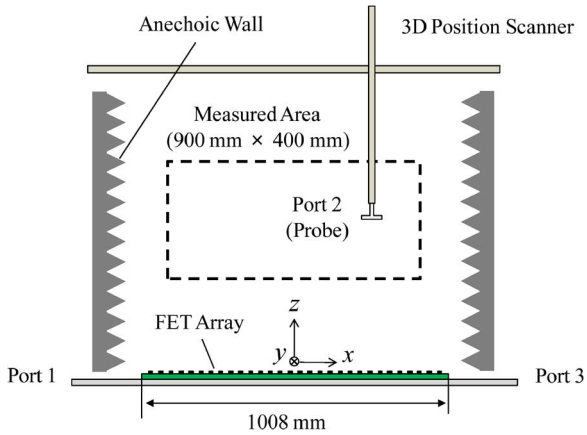

Fig. 6. Experimental setup. The measured area is indicated by the black broken rectangle.

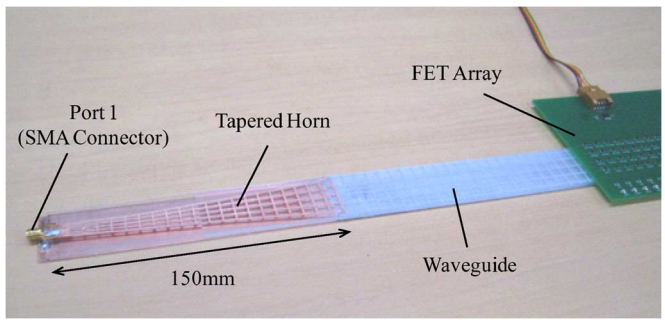

Fig. 7. Port 1 defined at the end of the tapered waveguide.

where α_n is a weight representing each scattering amplitude and $R_n(x,z)$ is the distance between the observation point and each scatterer given as

$$R_n(x,z) = \sqrt{(x-x_n)^2 + z^2}. \tag{8}$$

Since the scatterers constitute a non-uniform array, analytical calculation of (7) is difficult in general. When a focus is formed above the center of the aperture $(x_f \simeq 0)$, the focal width, w, can be roughly estimated from the following relation [19]

$$w \simeq \frac{\lambda_a z_f}{L} \tag{9}$$

where L is the length of the aperture and $\lambda_a (= 2\pi/k_a)$ is the wavelength in the air. Since a sharp spot is formed for $z_f \leq L$, the aperture length should be an order of 1 m for many indoor applications. For instance, (9) gives $w \simeq 62.5$ mm at $z_f = 500$ mm and $\lambda_a = 125$ mm (i.e. 2.4 GHz) when $L = 1$ m. Although the aperture length of the proposed antenna is basically determined by the physical length of the scatterer array, the effective aperture length would be a little smaller than that because scattering amplitude decays as the evanescent wave goes through energy leakage by the radiation and dielectric loss. Fig. 5 shows computed radiation patterns from (7) where α_n is assumed to be constant for simplicity. Here we designed (x_f, z_f) for (a) $(-300, 600)$ mm, (b) $(-50, 500)$ mm, and (c) (200, 900) mm with 15 pieces of scatterers aligned in nearly 1 m long according to (5) with $k_a = 50.2\ \mathrm{m}^{-1}$, $k_g = 88.5\ \mathrm{m}^{-1}$, and $x_0 = -484$ mm. The focal width, w, defined by $1/\sqrt{2}$ of the peak amplitude is (a) 99 mm $(= 0.79\lambda_a)$, (b) 74 mm $(= 0.59\lambda_a)$, and (c) 102 mm $(= 0.82\lambda_a)$. The sharpest width is attained in (b) since the focus is almost located above the center of the aperture and the aperture seen by the focus becomes largest in (b).

In the end of this section, we mention that the scatterer pattern becomes fully periodic when the focus is infinitely far from the aperture because (5) converges to a linear function of n as follows.

$$x_n \to \frac{2\pi n}{k_p} + x_0 \quad \left(\sqrt{x_f^2 + z_f^2} \to \infty\right) \tag{10}$$

where k_p is the wavenumber of the scatterer period given by

$$k_p = k_g - k_a \sin\theta \quad \left(\sin\theta \equiv \frac{x_f}{\sqrt{x_f^2 + z_f^2}}\right). \tag{11}$$

(11) is consistent with the following beamforming formula of conventional periodic leaky-wave antennas

$$\sin\theta = \frac{k_r}{k_a} \quad (k_r \equiv k_g - k_p) \tag{12}$$

where θ is the beam direction measured from z-axis and k_r is the wavenumber of the leaky wave. Thus, beamforming is equivalent to focusing toward an infinitely far focal point.

IV. Experimental Results

A. Device Fabrication

The fabricated structure is illustrated in Fig. 2. The waveguide layer is a quasi one-dimensional microstrip line composed of

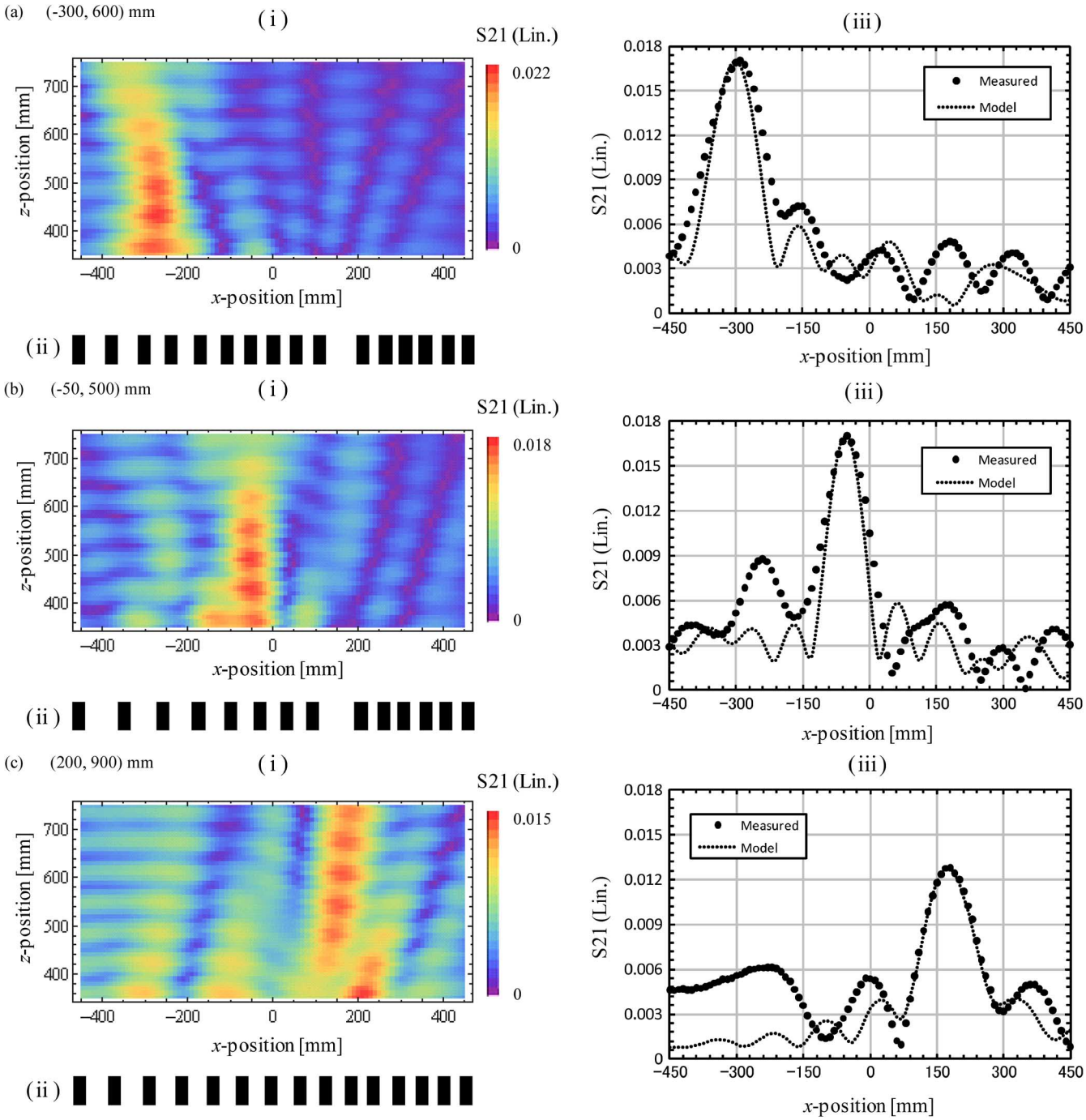

Fig. 8. Focus-scanning results. The focus was set at (a) $(x_f, z_f) = (-300, 600)$ mm, (b) $(-50, 500)$ mm and (c) (200, 900) mm. The measured S_{21} distribution and the programmed scatterer pattern at $y = 0$ mm are shown in (i) and (ii), respectively, sharing the same x-axis. (iii) shows the profile of (i) in the x-direction at $z = z_f$ for (a) and (b) and $z = 750$ mm (limit of the measured range) for (c).

a ground plane, a dielectric substrate, and a microstrip mesh. The dimensions are 1500 mm long in the x direction and 32 mm wide in the y direction. Both the ground plane and the microstrip mesh are made of aluminum printed on PET films. The microstrip mesh has a line width of 1 mm and a lattice period of 7 mm which is sufficiently smaller than the guided wavelength resulting in an inductive surface. The dielectric substrate is an acrylic plate of 3 mm thick with a relative permittivity of about 3. Although an acrylic plate is so lossy that more than 80% of the guided power is dissipated after 1500 mm propagation, we used it because of its availability and manufacturability in large dimensions.

The scatterer layer is composed of microstrip line-based cascade connection of FET source-drain channels supported on three jointed FR-4 substrates. Each substrate is 336 mm long and 2 mm thick with a relative permittivity of 4.9. On each surface, 160 pieces of commercial microwave FETs (SKY65050-372LF, SKYWORKS) are aligned in 40 cascaded columns and 4 parallel rows at 8 mm intervals in the x and y directions, respectively. In total, the three substrates constitute a scatterer layer of

1008 mm long on which 480 pieces of the FETs are aligned in 120 columns. All the source terminals of the FETs are grounded (0 V) with vertically printed thin lines as illustrated in Fig. 2(a). We confirmed that the vertical lines are uninfluential to the microwave transmission from numerical simulations. Note that the drain terminals are also grounded because they are connected to the next source terminals through short microstrip lines. The conductivities of the source-drain channels for microwave currents are switched by the gate-source voltages. The gate-source voltages of the 120 columns are switched independently (−3.3/0 V) with the other vertical lines and the voltages of the 4 rows are driven commonly.

B. Experimental Setup

The experimental setup is illustrated in Fig. 6. We defined port 1 at one tapered end of the waveguide (shown in Fig. 7) and port 2 at a standard dipole antenna (ASD-2425B, Antenna Giken) probing above the waveguide, and then measured the transmittance, S_{21}, at 2.4 GHz with a network analyzer (N5230A, Agilent). We also defined port 3 at the other end of the tapered waveguide and terminated it with an impedance matched resistor. The probe antenna was scanned with a 3D position controller (DM3474AV1, Device) surrounded by anechoic walls. The origin of the coordinate, $(x, y, z) = (0, 0, 0)$ mm, was defined at the center of the FET array, and the scanned ranges were $-450 \leq x \leq 450$ mm, $-400 \leq y \leq 400$ mm, and $350 \leq z \leq 750$ mm in each direction. The scanned area is indicated by a broken rectangle in Fig. 6. The scanning resolution was 10 mm ($\ll \lambda_a = 125$ mm at 2.4 GHz, where λ_a is the wavelength in the air). Since the radiated wave is transverse magnetic ($E_y = 0$), the probe dipole antenna was set along the x-direction during the measurement.

The guided wavelength, λ_g, was determined experimentally from the phase delay measurement through port 1 to port 3 when all the FETs were set off-state, and $\lambda_g = 71$ mm was obtained at 2.4 GHz. From this result, we determined to use 3 series of on-state FETs (resulting in a 32 mm line) as one scatterer identically to the previous simulation, and defined its x-position by the center of the 3 series. The scatterer pattern was programmed to a focus based on (5) where x_n was discretized by the FET array period (8 mm).

C. Focus Scanning

Fig. 8(i) shows the measured S_{21} distribution at $y = 0$ mm when the focus was set at (a) $(x_f, z_f) = (-300, 600)$ mm, (b) (−50, 500) mm and (c) (200, 900) mm. Field enhancement around the focus was clearly observed in all cases. Although z_f of (c) was out of the measured range, the field was obviously growing toward the focal point. Faint standing waves appeared in the z-direction probably because of the reflection by the 3D position scanner installed above. The programmed scatterer pattern is illustrated in (ii) sharing the same x-axis with (i). There is a lack of a scatterer around $x = 168$ mm in (a) and (b) because the location coincided with the substrate joint. The profile of Fig. 8(i) in the x-direction is plotted in Fig. 8(iii) where $z = z_f$ for (a) and (b), and $z = 750$ mm (limit of the measured range) for (c). The peak position agreed well to the aimed x_f with the error less than 10 mm $(0.08\lambda_a)$ in both (a) and (b). The focal width defined by $1/\sqrt{2}$ of the peak amplitude was (a) 120 mm $(0.96\lambda_a)$ and (b) 90 mm $(0.72\lambda_a)$. The dotted line plotted together with the measured data in (iii) was calculated from (7) and normalized to the measured peak. In the calculation, we assumed that the scattering amplitude, α_n, is constant with respect to n for simplicity. The model of (7) becomes less accurate off the peaks because it does not include the effects of other weak radiation such as scattering at the joints or the edges of FR-4 substrates.

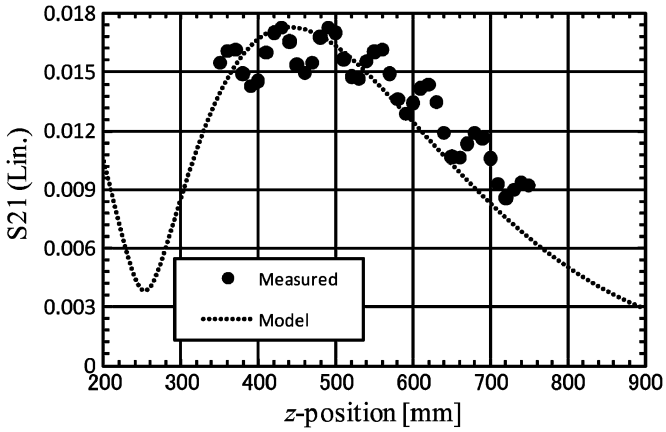

Fig. 9. Measured S_{21} in the z-direction at $x = x_f$ for $(x_f, z_f) = (-50, 500)$ mm.

Fig. 9 shows the profile of Fig. 8(b-i) in the z-direction at $x = x_f$. The dotted line was plotted based on the same model as above. The slight fluctuation of the measured values indicates the formerly mentioned standing waves. Actually, the distance between the antinodes was about 60 mm and corresponded to the half-wavelength in the air. The peaks of the measurement and the model slightly shifted below the aimed z_f (500 mm) because the scatterer pattern was designed based only on the phase relation in (3) and the factor of α_n/R_n in (7) was not into account, which becomes less accurate when the focus gets closer to the aperture. Although the measurement could not cover the entire profile in the z-direction, we estimated the focal depth to be about 260 mm $(2.1\lambda_a)$ from the model.

Since the scatterer array was almost one-dimensional, the focus was not formed in the y-direction. The result of probe scanning in the xy-plane at $z = z_f$ is plotted in Fig. 10 and the profile in the y-direction at $x = x_f$ is shown in Fig. 11. The focus spread about 600 mm in the y-direction. Fig. 10 also gives an estimation that roughly 10% of the input guided power was focused within the band of the focal width around $x = x_f$. More power can be focused by increasing the scatterer number with a longer FET array and decreasing the dielectric loss of the waveguide medium. These efforts are also effective in terms of sharpening the focus with a larger aperture. Fig. 12 shows focus shift accompanied by frequency variation. The focus at $x_f = -50$ mm at 2.4 GHz shifted −30 mm with 60 MHz decrease and +40 mm with 90 MHz increase. Finally, we mention that $S_{21} = S_{12}$ was satisfied during the measurement. Thus, the fabricated structure was shown to work reciprocally.

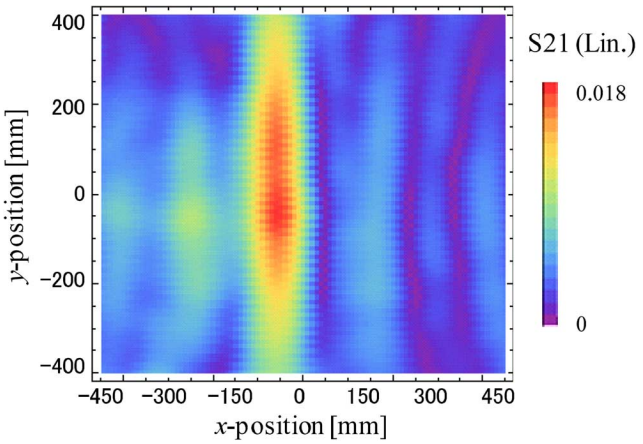

Fig. 10. Measured S_{21} in the xy-plane at $z = z_f$ for $(x_f, z_f) = (-50, 500)$ mm.

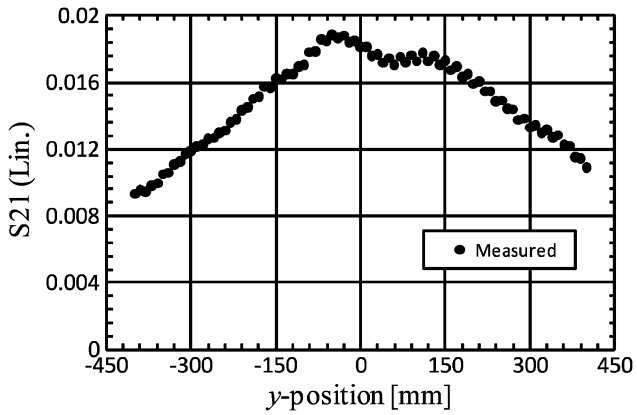

Fig. 11. Measured S_{21} in the y-direction at $x = x_f$ for $(x_f, z_f) = (-50, 500)$ mm.

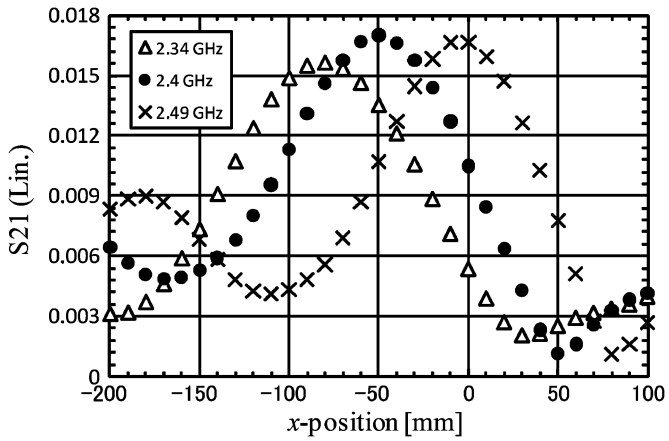

Fig. 12. Measured peak shift for $(x_f, z_f) = (-50, 500)$ mm accompanied by frequency variation.

V. Conclusion

A focus-scanning leaky wave antenna has been proposed. It is based on evanescent wave scattering by electronically reconfigurable microstrip array fabricated of FETs. Since each FET requires only a low voltage (−3.3 V) and leakage current ($\sim \mu$A) for its switching, the scatterer pattern can be programmed and reconfigurated by a simple electronic circuit with low power consumption. Our prototype has achieved focus-scanning at 2.4 GHz. The scanned range covers the measured area (900 mm × 400 mm) and a larger area measurement is required to evaluate the full scannable-range. The focal width was about one-wavelength at a distance of five-wavelength from the aperture. About 10% of the input power was focused while more than 80% was dissipated by the acrylic plate in the waveguide. The radiation efficiency will be increased by increasing the scatterer number with a longer FET array and replacing the waveguide medium with other low-loss materials such as PTFE. The longer array is also preferable in terms of sharpening the focus.

The proposed structure produces a very low-cost phased array. Promising applications include the use of phased arrays in indoor situations for smart wireless communication and sensing.

Acknowledgment

The authors thank H. Itai (Cellcross Co., Ltd.) for his technical support on the measurements.

References

[1] A. Buffi, A. A. Serra, P. Nepa, H. T. Chou, and G. Manara, "A focused planar microstrip array for 2.4 GHz RFID readers," *IEEE Trans. Antennas Propag.*, vol. 58, no. 5, pp. 1536–1544, Jan. 2010.

[2] S. Karimkashi and A. A. Kishk, "Focused microstrip array antenna using a Dolph-Chebyshev near-field design," *IEEE Trans. Antennas Propag.*, vol. 57, no. 12, pp. 3813–3820, Dec. 2009.

[3] K. D. Stephan, J. B. Mead, D. M. Pozar, L. Wang, and J. A. Pearce, "A near field focused microstrip array for a radiometric temperature sensor," *IEEE Trans. Antennas Propag.*, vol. 55, no. 4, pp. 1199–1203, Apr. 2007.

[4] M. Bogosanovic and A. G. Williamon, "Microstrip antenna array with a beam focused in the near-field zone for application in noncontact micowave industrial inspection," *IEEE Trans. Instrum Meas.*, vol. 56, no. 6, pp. 2186–2195, Dec. 2007.

[5] Y. Monnai and H. Shinoda, "Microwave phased array sheet for wireless sensor network," in *Proc. 7th Inte. Conf. on Networked Sensing Systems (INSS2010)*, Kassel, Germany, Jun. 2010, pp. 123–129.

[6] K. L. Klohn, R. E. Horn, H. Jacobs, and E. Freibergs, "Silicon waveguide frequency scanning linear array antenna," *IEEE Trans. Microwave Theory Tech.*, vol. 26, no. 10, pp. 764–773, Oct. 1978.

[7] F. K. Schwering and S. T. Peng, "Design of dielectric grating antennas for millimeter-wave applications," *IEEE Trans. Microwave Theory Tech.*, vol. 31, no. 2, Feb. 1983.

[8] M. Guglielmi and D. R. Jackson, "Broadside radiation from periodic leaky-wave antennas," *IEEE Trans. Antennas Propag.*, vol. 41, no. 1, Jan. 1993.

[9] H. Maheri, M. Tsutumi, and N. Kumagai, "Experimental studies of magnetically scannable leaky-wave antennas having a corrugated ferrite slab/dielectric layer structure," *IEEE Trans. Antennas Propag.*, vol. 36, no. 11, pp. 911–917, Nov. 1988.

[10] V. Varadan, V. V. Varadan, K. A. Jose, and J. F. Kelly, "Electronically steerable leaky wave antenna using a tunable ferroelectric material," *Smart Mater. Struct.*, vol. 3, pp. 470–475, Jun. 1994.

[11] J. B. L. Rao, G. V. Trunk, and D. P. Patel, "Two low-cost phased arrays," *IEEE AES Syst. Mag.*, pp. 39–44, Jun. 1997.

[12] D. Sievenpiper, "Forward and backward leaky wave radiation with large effective aperture from an electronically tunable textured surface," *IEEE Trans. Antennas Propag.*, vol. 53, no. 1, Jan. 2005.

[13] L. Huang, J. Chiao, and P. Lisio, "An electronically switchable leaky wave antenna," *IEEE Trans. Antennas Propag.*, vol. 48, no. 11, pp. 1769–1772, Nov. 2000.

[14] S. Lim, C. Caloz, and T. Itoh, "Metamaterial-based electronically controlled transmission-line structure as a novel leaky-wave antenna with tunable radiation angle and beamwidth," *IEEE Trans. Microwave Theory Tech.*, vol. 53, no. 1, Jan. 2005.

[15] C. T. Rodenbeck, M. Li, and K. Chang, "Design and analysis of a reconfigurable dual-beam grating antenna for low-cost millimeter-wave beam-steering," *IEEE Trans. Antennas Propag.*, vol. 52, no. 4, Apr. 2004.

[16] R. Ulrich, "Far-infrared properties of metallic mesh and its complementary structure," *Infrared Phys.*, vol. 7, no. 1, pp. 37–55, 1967.
[17] H. Shinoda, Y. Makino, N. Yamahira, and H. Itai, "Surface sensor network using inductive signal transmission layer," in *Proc. 4th Inte. Conf. on Networked Sensing Systems (INSS2007)*, Jun. 2007, pp. 201–206.
[18] K. R. Carver and J. W. Mink, "Microstrip antenna technology," *IEEE Trans. Antennas Propag.*, vol. 29, no. 1, pp. 2–24, Jan. 1981.
[19] R. C. Hansen, "Focal region characteristics of focused array antennas," *IEEE Trans. Antennas Propag.*, vol. 33, no. 12, pp. 1328–1337, Jan. 1985.

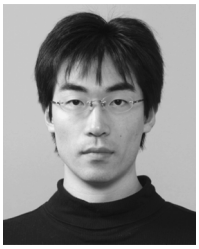

Yasuaki Monnai (S'10) received the B.S. degree in mathematical engineering and information physics and the M.S. degree in information physics and computing from the University of Tokyo, Tokyo, Japan, in 2008 and 2010, respectively, where he is currently working toward the Ph.D. degree.

He is a Research Fellow of Japan Society for the Promotion of Science. His research interest includes controlling wave propagation by designing the structure or morphology of transmission systems and applying them to wireless communication, measurements, and human-machine interfaces.

Mr. Monnai is a student member of IEICE, and SICE.

Hiroyuki Shinoda (M'95) received the B.S. degree in applied physics, the M.S. degree in information physics, and the Ph.D. degree in electrical engineering from the University of Tokyo, Tokyo, Japan, in 1988, 1990, and 1995, respectively.

In 1995, he was a Lecturer and in 1997 an Associate Professor in the Department of Electrical and Electronic Engineering, Tokyo University of Agriculture and Technology. He was a Visiting Researcher at UC Berkeley in 1999. Since 2000, he has been an Associate Professor in the Graduate School of Information Science and Technology, University of Tokyo. His research interest includes information physics, tactile/haptic interfaces, sensor systems and devices, sensor networks, two-dimensional communication, human interfaces, and optical/acoustic measurement.

Dr. Shinoda is a board member of SICE and a member of IEEJ, RSJ, VRSJ, and JSME.